Journal of the Meteorological Society of Japan

EARLY ONLINE RELEASE

The DOI for this manuscript is
DOI:10.2151/jmsj.2022-028
J-STAGE Advance published date: March 10th, 2022
The final manuscript after publication will replace the preliminary version at the above DOI once it is available.

The roles of local circulation and boundary layer development in tracer transport over complex topography in central Taiwan

Min-Ken HSIEH

Department of Atmospheric Sciences, National Taiwan University, Taipei, Taiwan

Central Weather Bureau, Taipei, Taiwan

Yu-Wen CHEN

Research Center for Environmental Change, Academia Sinica, Taipei, Taiwan

Yi-Chun CHEN

Research Center for Environmental Change, Academia Sinica, Taipei, Taiwan

and

Chien-Ming WU[1]

Department of Atmospheric Sciences, National Taiwan University, Taipei, Taiwan

February 1, 2022

----

1) Corresponding author: Chien-Ming WU, No. 1, Sec. 4, Roosevelt Rd., Taipei 10617, Taiwan (R.O.C.).

Email: mog@as.ntu.edu.tw

Tel: +886-2-3366-3905

Fax: +886-2-2363-3642

Abstract

We applied tracer transport simulations using Taiwan vector vorticity equation cloud-resolving model (TaiwanVVM) to evaluate the effects of the local circulation associated with the lee vortex and the planetary boundary layer development on the transport and accumulation of the pollutants on a diurnal time scale in central Taiwan. The wind directions of crucial synoptic northeast monsoon are idealized as the initial conditions of the simulations to examine the impact of the lee vortex on the pollutants transport. The primary local non-traffic emission sources are taken as the tracer emission sites so that the experiment results could be a good proxy of the realistic scenarios. With the local circulation over complex topography being resolved explicitly, the impact of the boundary layer development on the tracer transport of the Puli basin is discussed. The simulation results clarify the contribution of the sea breeze and the lee vortex to the tracer transport in central Taiwan. We conclude that high tracer concentration at Puli at night is due to the tracer being trapped by the thinning of the mixed layer depth in the evening. The sensitivity of the local tracer transport to the change of the synoptic wind direction shows that under northeasterly due east (due north) environment, the pollutant transports from the southern source (northern source) of central Taiwan are most likely to induce high concentration in Puli at night. This is the first study to distinguish the

contribution of the sea breeze and the lee vortex in pollutants transport in Taiwan. The results obtained from idealized experiments provide the possible mechanism of pollutants transport, which could be taken as an insight to interpret the observations and guide the design of field experiment to further establish the fundamental principles of the pollution transports in central Taiwan.

Keywords: pollutant transport, local circulation, lee vortex, planetary boundary layer, large eddy simulation

1. Introduction

The fine particulate matter ($PM_{2.5}$; particles with a diameter of 2.5 micrometers or less) pollution is a serious environmental issue in Taiwan. Several studies conducted in Taiwan discussed the possible pollutants transport mechanism associated with the local circulation: Tsai et al. (2008) investigated the influences of the land-sea breeze on the transport of gaseous air pollutants around the coastal region of Southern Taiwan. They showed that ambient air pollutants could be transported back and forth across the coastline by the land-sea breeze. Hsu and Cheng (2016, hereafter HC16) showed that the pollution on the west plain of Taiwan is prone to be high under the land-sea breeze embedded in the weak synoptic weather during wintertime. While these studies emphasized the role of the land-sea breeze on the pollutants transport under the weak synoptic weather, the high aerosol concentration distributed on the leeside of the central mountain range of Taiwan under the prevailing winds also came to attention. Chuang et al. (2008) pointed out that while the weak winds and the high atmospheric stability are crucial factors to promote the high aerosol concentration in the Taipei basin, the terrain blocking effect on the leeside of the prevailing winds could also cause aerosol accumulation. Hsu and Cheng (2019) also showed that southwestern Taiwan situated on the leeside of the central mountain range often exhibits the worst air pollution under the prevailing northeasterly monsoon. These studies suggested that the interaction between the topography of Taiwan and the prevailing wind should be taken into account when inspecting the pollutants' transport mechanism. Lai and Lin (2020, hereafter LL20) further proposed that the lee vortex, which is induced by the prevailing winds blocked by the central mountain range of Taiwan, is a crucial factor to the pollutant transport mechanism in Taiwan. After inspecting the composite of more than 300 simulations of the pollution events and the aerosol concentration observation, they concluded that the location of the induced lee vortex is sensitive to the pitching angle of prevailing winds, which is defined as the angle between the axis of the central mountain range and the prevailing wind direction. The location of the lee vortex and its evolution consequently impact the areas of the severe pollution areas in the island scale, such as in central or southern Taiwan. Despite the importance of the lee vortex to the local pollutant distribution in Taiwan claimed by LL20, there is little observation examination of the lee vortex under the high pollution events in their study. The existence of the lee vortex could be clearly identified in some pollution cases of Taiwan (see Appendix as an example), which implies that the crucial pollutants transport mechanism should be associated with the lee vortex. However, it is challenging to clarify the transport contribution by the lee vortex in the observation considering that the local $PM_{2.5}$ is the result of the pollutants being transported from all kinds of emission sources in Taiwan. In this study, a large-eddy simulation approach is employed to evaluate the effects of the lee vortex on the pollutants transport and to identify possible emission sources responsible for the local pollutant distribution under the synoptic condition revealed by HC16 and LL20.

While the aforementioned studies indicated the importance of the local circulation associated with the land-sea breeze and the lee vortex on the pollutants transport, the evolution of the local circulation under different prevailing wind directions and its impact on the pollutants transport are still not clear. The contribution of the land-sea breeze and the lee vortex to the pollutants transport under different synoptic conditions also need to be examined quantitatively. Moreover, the distribution of the pollutants discussed in these studies mainly focused on the plain areas of Taiwan. Regarding the mechanism of the pollutants transport and accumulation over the mountain area, the local circulation associated with the topography, such as the mountain valley wind system, could also play a role in the pollutants transport, which is rarely discussed before. The details of the aerosol concentration distribution across the plains and mountain areas are also interesting. For example, HC16 also pointed out that the Puli site, a basin situated at the mountain area of the central mountain range, recorded the second-highest average $PM_{2.5}$ concentration from the year 2014-2015. Since the non-traffic pollution sources such as chemical industry factories and power plants are primarily located in the coastal area, the mechanism of the pollutants transported to and accumulated in the Puli basin is worthy of being further investigated.

Considering the pollutants transport and accumulation over complex topography, the vertical dispersion of the pollutants related to the characteristics of the planetary boundary layer (PBL) development is also a key factor in determining the local pollutant concentration. Chang et al. (2006) analyzed the microwave temperature profiler data of the pollution episodes in Taiwan. They suggested that the mixed layer depth and its diurnal variation are essential to the evolution of local pollution. The local pollutant concentration is modulated by the local flow and the vertical mixing processes simultaneously. In the Puli basin, which is located on the west side of the central mountain range with complex surrounding topography, the PBL development should be carefully evaluated to clarify its role in pollutant transport.

In this study, we aim to understand the mechanism responsible for the local circulation that causes high pollutant concentration at the Puli basin using idealized simulations. As Lesouef et al. (2011) demonstrated, the idealized numerical experiment is suitable to investigate the local scale transport and dispersion of pollutants emitted from local sources in the context of a uniform maritime flow obstructed by a mountainous island.

Arnold et al. (2012a, 2012b) showed that the modeling framework with nested-domain generally causes problems over complex topography, including the noise produced at the nest boundaries, the spin-up needed for the high-resolution domain, and the boundary of the nested domain. To avoid these issues, the domain boundaries of the numerical simulation should be far enough from the region of interest. In this study, a high-resolution (500 m) single domain covering the whole of Taiwan is used in the numerical simulation framework to simulate the local circulation and PBL development over complex topography in Taiwan. The high horizontal resolution single domain design is to avoid the nested-domain simulation problems mentioned above meanwhile still capable of capturing flow around ridges and valleys of Taiwan. A series of idealized tracer transport simulations are carried out to clarify the roles of the land-sea breeze and the lee vortex on the transport of pollutants to the Puli basin. The tracer emission sites are configured on the west coast of Taiwan to evaluate the tracer transport processes on the west plain of Taiwan. In PBL, high vertical resolution (100 m) within 4 km is used to better capture the evolution of PBL development. In our experiments, the synoptic northeasterly monsoon with different prevailing wind directions is also considered in the tracer transport simulations to discuss the evolution of the lee vortex under different synoptic conditions in the distribution of the tracer concentration. The goals of this study are: 1) to identify the role of the lee vortex in the tracer transport mechanism; 2) to evaluate the impact of the prevailing wind direction of northeasterly monsoon on the evolution of the lee vortex circulation; and 3) to understand how the local tracer concentration at Puli be modulated by the development of the PBL and the local circulation. The statistic of the observation data is presented in section 2. The model and the experiment design are presented in section 3, which includes the description of TaiwanVVM and the numerical setup of the idealized simulations. The examination of the simulation results is presented in section 4, in which the mechanism associated with the lee vortex and the development of the PBL is discussed. A summary and discussion are given in section 5.

2. Observational Basis

Inspired by LL20, we first analyze the relationship between the prevailing winds and the pollution of central Taiwan in the observations. We follow the definition of the prevailing winds in LL20 and take the winds of the lowest level in the sounding data at Ishigakijima of Japan at 00:00 UTC of each day to represent the synoptic winds. Figure 1 shows the geographic locations of Taiwan and Ishigakijima (yellow asterisk), as well as the major local non-traffic emission sources (red squares, Taichung Power Plant (TPP), and Sixth Naphtha Cracker (SNC)) and the observation sites (blue triangles, Zhushan and Puli) in central Taiwan we focused on in this study. It is worth noting that the Puli basin is on the west side of the central mountain range. The height of the surrounding mountains of the Puli basin ranges from 800 to 2000 m. Zhushan is situated at the fringe of the western plain of Taiwan, which is also next to the foothill of the central mountain range. Figure 2 shows the windroses of the synoptic winds in 2005-2015. While the day-by-day prevailing wind directions can vary from northeasterly due north (NNE) to southerly as shown in Fig. 2a, the wind directions are mostly confined between 20° to 80° when only considering the pollution days at Puli (Fig. 2b). Figure 2b also shows that the highest frequency of the pollution days at Puli is under the NNE synoptic winds and followed by the northeasterly (NE) and northeasterly due east (ENE) winds. The windroses indicate that although the west plain of Taiwan is mainly under the weak wind condition during the northeasterly monsoon, which favors the pollution transport by the land-sea breeze as suggested by HC16, the slight change of the synoptic wind direction still impacts the pollution of the Puli basin. The sensitivity of the Puli pollution days to the synoptic wind direction also implies that the local circulation associated with the lee vortex could result in the different pollutants transport scenarios on a finer scale than LL20 suggested.

To elaborate on the characteristics of the pollution distribution associated with the local circulation in central Taiwan, we further choose Zhushan along with Puli as the examining sites of the aerosol concentration and the local flow in this section. As HC16 pointed out, the major non-traffic emission sources are located in the coastal area, and the land-sea breeze could promote the pollutants being transported inland. Under this circumstance, Zhushan is taken upstream of the Puli basin when examining the transport processes of the pollutants emitted from the coastal area. Figure 3 shows the diurnal variations of the aerosol concentration and the local winds at Zhushan and Puli of the composite of the 310 pollution days at Puli from 2005 to 2015. Figure 3a shows that there is a profound diurnal cycle of the aerosol concentration at both Zhushan and Puli. The timing of the highest concentration at Zhushan is at 18:00 LST while it at Puli is 3 hours later, which indicates that the pollutants could be transported from plain to mountain area by sea breeze as HC16 suggested. The aerosol concentration at Puli at night is higher than the highest concentration at Zhushan, which indicates that the processes of the pollutants accumulation could be another important factor to explain the pollution at Puli. While the profound diurnal variation and the high concentration at Puli at night could be attributed to the decrease of the PBL height after sunset, the stronger diurnal variation amplitude of the concentration at Puli compared with that at Zhushan indicates that the impact of the PBL development on local pollutants accumulation could be different between plain and mountain areas, which is worthy of being further evaluated by numerical simulation. The signature of the sea breeze is also evident in Fig 3b. Considering the coastline is west of the plains and mountain areas in central Taiwan, the robust westerly in the daytime at Zhushan and Puli is due to the sea breeze initiates and develops from the coastal area to the plain and mountain areas.

Figure 3b also shows that the land breeze is weak at night compared to the sea breeze. The westerly sea breeze in the daytime accompanied with mild northerly is shown in Fig. 3c, which might be associated with the slant coastline as shown in Fig. 1. The characteristics and evidence of the local circulation associated with the lee vortex are little discussed in the aforementioned studies, which is probably because that the sea breeze signature is much profound in the composite of the observation as we shown in Figs. 3b and 3c. Since the formation of the lee vortex and its movement results in a varying flow pattern locally, it is difficult to evaluate the lee vortex by the mixed results of the local winds at a single point. However, it is worth noting that the deviation from the composite meridional wind in Fig. 3c indicates that the day-to-day meridional wind of the local flow could change from northerly to southerly in the pollution days at Puli. The variability of the meridional wind component could be taken as the consequences of the local circulation modulated by the lee vortex, which is not a uniform flow but tends to change the directions along with the cyclonic circulation of the lee vortex. To clarify the contribution of the land-sea breeze and the lee vortex to the pollutants transport as well as the effects of the PBL development on the pollutants accumulation, we performed a series of idealized tracer transport experiments. In contrast to the case study, the initial synoptic winds are idealized to three different uniform flows according to the windrose in Fig. 1 to better understand the tracer transport and accumulation processes. The examination of the tracer transport mechanism in the simulations and the numerical experiment setup are presented in the next section.

3. Model and experiment design

3.1 TaiwanVVM

It is very challenging for numerical models to simulate the pollution transport over the complex topography using PBL schemes that are designed in one dimension or flat surfaces (Goger et al. 2018, 2019). Using different PBL schemes in the model could influence both the strength of the land-sea breeze and the PBL height, consequently resulting in different concentrations of the pollutants in Taiwan (Cheng et al. 2012).

In this study, we use TaiwanVVM following Wu et al. (2019) and Chang et al. (2021) to capture the tracer transport in the boundary layer. Idealized simulations in these studies help understand the fundamental mechanisms associated with flow over complex topography in Taiwan. TaiwanVVM uses high horizontal (500 m) and vertical (100 m) resolution with simple eddy diffusion turbulence closure to explicitly simulate the PBL development over complex topography. In addition, the Noah land surface model (LSM) is implemented in TaiwanVVM with corresponding realistic land surface data of Taiwan (Wu et al. 2019). A unique aspect of the TaiwanVVM is that the model predicts the horizontal components of vorticity and diagnoses the vertical velocity using a three-dimensional elliptic equation (Jung and Arakawa 2008). Therefore, the pressure gradient force is eliminated, and the horizontal vorticities can respond directly to the buoyancy force to better capture the local-scale circulations associated with the substantial heating difference, such as the land-sea breeze or mountain-valley wind system. The complex topography with steep slopes in Taiwan is modeled through the immersed boundary method in height coordinate (Wu and Arakawa 2011; Chien and Wu 2016), which allows us to simulate the interaction between prevailing winds and the topography such as lee vortex. This model has been used to study the unified parameterization for deep convection (Arakawa and Wu, 2013; Wu and Arakawa, 2014), stratocumulus transition (Tsai and Wu, 2016), aggregated convection (Tsai and Wu, 2017; Chen and Wu, 2019), and afternoon thunderstorms over complex topography (Kuo and Wu, 2019; Wu et al., 2019; Chang et al., 2021). The detailed TaiwanVVM setup in this study is presented in Table 1, which follows the numerical setup in Chang et al. (2021) except for the initial condition.

3.2 Idealized experiments

The idealized experiment aims to isolate the most crucial mechanism governing the distribution of the pollutant on the west plain of Taiwan. Therefore, the synoptic environment is idealized as the initial condition with a uniform background flow over the whole domain so that we can focus on the interactions between the lee vortex and the local circulation. Figure 4 shows the initial condition of the simulation. The potential temperature, water vapor mixing ratio, and wind profiles are set to a typical winter condition, which is idealized from the sounding data upstream of Taiwan at Ishigakijima of Japan at 00 UTC on Dec. 21, 2017, as shown in Figs. 4a and 4b. The environment is stable with moderate moisture below 2000 m. We smooth the strength of the inversion in the idealized initial conditions to represent the general stratification characteristics of the atmosphere around Taiwan under northeasterly monsoon in the winter. The stratified atmosphere prohibits the vertical mixing of the pollutants by the synoptic-scale forcing. The distribution of the pollutants could only rely on the local circulation and the vertical eddy mixing initiating from the surface. To inspect the mechanism of the different prevailing wind directions resulting in the observation statistics obtained in Fig. 1, we idealized the initial near-surface background flow to 20°, 50°, and 80° (NE20, NE50, and NE80) uniformly in the horizontal domain. The initial wind profiles below 3000 m in these three experiments are shown in Figs. 4c, 4d, and 4e to emphasize the different prescribed northeasterly monsoon wind directions on the lowest 850 m. The specific wind directions are then veering upward to the westerly at the level of 3000 m in the initial condition of the simulation to represent the typical shallow northeasterly monsoon wind fields near Taiwan. For inspecting the land-sea breeze evolution and the PBL development over Taiwan's topography within a diurnal time scale, the simulations initiate at 6 AM of the local standard time (LST), which is 2 hours prior to the sounding data we idealized from, and are integrated for 18 hours. We take the first 2 hours as the spinning up period, and the simulation results from 8 LST (00 UTC) to midnight (24 LST) are examined to understand the tracer transport associated with the local effects.

To better understand the details of the local tracer transport under the blocked northeasterly monsoon synoptic condition, we focus on the simulation results in central Taiwan. The tracer emission sites are configured on the coastal area of central Taiwan, which are Taichung Power Plant (TPP) and Sixth Naphtha Cracker (SNC), as shown in Fig. 1. These sites represent the major local non-traffic emission sources of central Taiwan so that our idealized experiment results could be a good proxy of the realistic scenarios. The tracer site's emission is normalized to unity at 100 m above the ground every time step. The tracers could then be transported with the local circulation under the blocked northeasterly monsoon flow. The tracers are considered as gaseous emission, and therefore the deposition is ignored in the simulations.

In the following analyses, we first examine the local circulation starts from an island scale (~100 km) to identify the lee vortex under different initial background wind directions. The domain is then zoomed into central Taiwan (as the area shown in Fig.

1) to inspect the tracer transport processes associated with the local circulation and the resulting evolution of the tracer concentrations in Zhushan and Puli. The PBL development and the local flow pattern are then analyzed to discuss how the diurnal variation of the PBL development and the flow over complex terrain impact the local tracer concentrations.

4. Simulation results

4.1 Local circulation associated with the lee vortex under the northeast monsoon

The simulation results show that the slight change of the northeasterly monsoon wind direction leads to the different scenarios of the lee vortex evolution and modulates the local circulation. Figure 5 presents the characteristics of the local circulation associated with the lee vortex in three experiments at noon (12:00 LST) and night (22:00 LST). It shows that from NE20 to NE80, the blocking effects of the central mountain range become stronger, and consequently, the lee vortex becomes more profound. In NE20, the background synoptic flow is mostly parallel with the axis of the central mountain range so that there are few blocking effects of the central mountain range. The local circulation is mainly composed of the synoptic northeasterly monsoon flow and the sea breeze induced locally in the daytime (Fig. 5a). While the characteristics of the sea breeze is profound at noon in NE20, the flow turns to several small vortices on the plain area at 22:00 LST (Fig. 5d), which indicates that the local circulation becomes rather weak and more turbulent at night and there is little evidence of the land breeze at night. The signature of the uneven strength of the land-sea breeze is consistent with the observation shown in Fig. 3b earlier. With the increase of the easterly component of the background flow, the local circulation is no longer only attributed to the sea breeze and the synoptic flow. The local circulation of NE50 at 12:00 LST (Fig. 5b) shows that a cyclonic swirl stretches along the coastline, and the stretching swirl results in a rather profound southerly wind on the west plain of Taiwan compared to NE20. The southerly proceeds at night, as shown in Fig. 5e, which is evident that the central mountain range's mild blocking effect can impact the local circulation even when the lee vortex is difficult to identify. In NE80, the lee vortex is identified under the strongest blocking effects among the experiments. Figure 5c shows that two lee vortices are located at the northwest coast and the southwest sea of Taiwan at noon. The northern one then moves offshore toward the north of Penghu island, while the southern one moves westward out of the domain throughout the day (Fig. 5f). As the lee vortices form at noon, the circulation associated with the lee vortices dominates the local circulation. It shows that the lee vortex induces the profound westerly in central Taiwan at noon. With the northern lee vortex moving southwestward, the local flow in central Taiwan turns southerly at night.

To evaluate the impact of the lee vortex on the local circulation, we further inspect the evolutions of the mean 10 m winds in the plain area of central Taiwan in all experiments (Fig. 6). While the characteristics of the intensified westerly in the daytime, which is consistent with the observational analysis, exist in all the experiments (Fig. 6a), the mechanism behind these phenomena could be different among these three experiments. As shown in Fig. 5c, the westerly in the daytime in NE80 is mainly due to the circulation associated with the lee vortices. The combination of the cyclonic flow of the north vortex and the anti-cyclonic circulation of the south vortex leads to a robust westerly in central Taiwan. The local winds vary along with the drifting of these lee vortices. After the southern vortex moves out of the domain, the local flow in central Taiwan is controlled solely by the northern lee vortex offshore (Fig. 5d). The weakening of the westerly at night is because the local flow veers from westerly to the south-southwesterly (SSW) as the vortex moves from north to west to central Taiwan. In contrast, the westerly in NE20 and NE50 is most likely attributed to the sea breeze in the daytime. The cease of the sea breeze in these two experiments at night also agrees with the observation. Figure 6a also indicates that the intensity of the westerly induced by the lee vortex, which reaches 2.5 m s^{-1} at 14:30 LST, is generally about 1 m s^{-1} stronger than the westerly induced by the sea breeze. The maximum westerly in NE20 and NE50 is about 1.5 to 2 m s^{-1}, which is comparable to the observation shown in Fig.

3b. Regarding the evolution of the meridional component of the mean surface winds in the plain of central Taiwan, the results among these three experiments show more variability (Fig. 6b). It shows that even the meridional winds are similar in the first few hours after spin-up, the evolutions of the meridional winds are distinctly different under the different blocking effects of the central mountain range. The sustained northerly wind throughout the day in the NE20 experiment indicates that there are few changes from the prevailing northeasterly monsoon when only considering the meridional flow in central Taiwan. As the northeasterly monsoon veers to easterly with stronger blocking effects, it shows that the northerly wind turns southerly along with the leeside effects in the plain area of central Taiwan. Figure 6b shows that the initiation of the southerly is as early as 14:00 LST in NE80, and it delays for 6 hours in NE50. Considering the center of the lee vortex is mostly located on the coastal area or over the sea, the southerly on the plain area is due to the cyclonic circulation of the north lee vortex. The modeling results indicate that the crucial impact of the different leeside effects on the local circulation is the timing of the initiation of the southerly in the plain of central Taiwan. With the synoptic flow veering from NNE to ENE, the leeside effect is getting more apparent. The blocking effect of the central mountain range under different northeasterly monsoon wind directions changes the timing of the lee vortex formation. It modulates the evolution of the local circulation, which leads to the local tracer concentration at Zhushan and Puli being sensitive to the prevailing wind directions. In the next subsection, we elaborate on the tracer transport scenarios at Zhushan and Puli to clarify the roles of the local circulation on the modulation of the local tracer concentration at Puli.

4.2 Tracer transport processes in central Taiwan

We first present the time evolution of the tracer concentration in Zhushan and Puli in Fig. 7. Within only 40 km between TPP and SNC, the transport downstream in Zhushan and Puli has distinct different evolution under similar background environments. Besides, relative high tracer concentration exists in Puli at night in NE20 (NE80) from TPP (SNC). Regarding the tracer transport from TPP, the peak time of pollution concentration at Zhushan/Puli tends to delay as the synoptic wind veers toward northerly anti-clockwise. Their concentrations are also higher (Fig. 7a). The peak time at Puli is always 2.5 to 3.5 hours later than Zhushan because Zhushan is upstream to Puli when the tracer is transported from TPP to the mountain area by the westerly. In NE80, the peak time can be as early as 11 AM at Zhushan, and in NE20, it delays for 2 hours, which is due to the weaker westerly shown in Fig. 6a. After the peak time at Zhushan/Puli, the tracer concentration decreases quickly in NE50 and NE80, while in NE20, the concentration at Zhushan decreases slowly after reaching its peak at 13:00 LST. When the concentration at Puli reaches its peak at 16:30 LST, the TPP tracer concentration at Zhushan even increases slightly. The concentrations at Zhushan then decrease after 17:30 LST while it at Puli remain higher than 0.005 throughout the day. The overall concentration at Zhushan/Puli after 18:00 LST is higher compared with it in NE50 or NE80.

The time evolution of the tracer transport from SNC is distinctly different from TPP in that only NE50 and NE80 can reach Zhushan, and only NE80 can reach Puli (Fig. 7b). In addition, the timing of tracer transport from SNC approaching Zhushan and Puli is generally later than that from TPP. In NE80, the peak time of the SNC tracer concentration at Zhushan is at 15:30 LST, while it is at 18:30 LST in NE50. The downstream relationship between Zhushan and Puli does not exist in NE50 regarding tracer transport from the SNC, which indicates that in addition to local circulation, the diurnal evolution of the PBL could also play an important role. To further demonstrate the tracer transport scenarios in central Taiwan, we examine the evolution of the tracer concentration along with the local circulation development. The results show that the streak structure of the tracer concentration follows the local circulation before entering the mountain area. Figure 8 shows the evolution of the surface concentration of the tracer emitted from TPP in three experiments. In the morning (11:00 LST), the lee vortex promotes the earlier eastward transport of the tracer. This feature can be visualized in the NE80 experiment in which the streak structure of the tracer reaches the east of TPP (Fig. 8c), while in other experiments, the tracer streak spreads southward (Figs. 8a and 8b). In the afternoon (14:00 LST), the lee vortex north to TPP in the NE50 experiment (Fig. 8e) also induces the southwesterly flow to transport tracer northeastward. The tracer distribution in NE50 and NE80 shows that when the primary tracer streak swipes quickly following the cyclonic circulation associated with the lee vortex, the tracer concentration in the mountains around Puli stays relatively low values at 18:00 LST (Figs. 8h and 8i), compared with the high tracer concentration at Puli in the NE20 experiment (Fig. 8g). In NE20, the tracer concentration increases dramatically as the tracer transports into the mountain area, and it is the highest among all experiments at night at Zhushan and Puli in NE20 (Fig. 7a), which can be related to the PBL development as discussed in the following subsection.

Figure 9 shows the evolution of the surface tracer concentration emitted from SNC in the three experiments. Although the evolution of the lee vortex is identical, the location of SNC (40 km south of TPP) prevents the direct influence from the lee vortex. The tracer transport from SNC is mostly southward and southeastward from 11:00 (Figs. 9a, 9b, and 9c) to 14:00 (Figs. 9d, 9e, and 9f) LST. In the NE20 experiment (Figs. 9a, 9d, and 9g), the tracer from SNC is transported southward by the coastal northeasterly monsoon flow. The sea breeze only spreads the tracer eastward slightly at 18:00 LST, and the tracer cannot reach Zhushan and Puli in the whole simulation. The result is in sharp contrast to tracer transport from TPP simply due to the location of the lee vortex. The cyclonic circulation in NE50 and NE80 is evident in the evening (Figs. 9h and 9i) and promotes the tracer transported eastward. In the NE80 experiment (Figs. 9c, 9f, and 9i), the local circulation around SNC turns eastward the earliest in the morning, and the flow veers to the northeastward in the evening, which leads to the direct transport of the tracer to the mountain area produces high tracer concentration at Puli.

The examination of the horizontal tracer distribution shows that the local circulation controls the timing of the streak structure of the tracer approaching Zhushan and Puli, as demonstrated in Fig. 7. The timing of the tracer transported to the mountains further impact the local concentration evolution at night. To interpret the variation of the tracer concentration at Zhushan and Puli at night, we analyze the development of the PBL and discuss its impacts on tracer transport and accumulation in the next subsection.

4.3 Impact of the thinning of mixed-layer depth in the evening

While the local circulation associated with the lee vortex impacts the tracer transport scenarios, the development of PBL also plays a role in the modulation of the trace concentration at Puli. There are several approaches to estimating PBL depth. In this study, we use a simple well-mixed assumption to estimate the mixed-layer depth as an index to describe the diurnal evolution of PBL. The mixed-layer depth is defined as the depth at which the potential temperature equals the surface potential temperature plus 0.5 K. This definition links the mixed-layer depth to solely the near-surface potential temperature profile so that the mixed-layer depth could be a good indicator of the activity of the thermals initiated by the surface heating in the daytime. A clear diurnal cycle of the mixed-layer depth exists for both Zhushan and Puli in all the experiments (Figure not shown). As demonstrated in the last subsection, the local circulation under different strengths of the blocking effect results in the different TPP tracer transport scenarios. Due to the variation of the lee vortex in these experiments, the timing of the tracer streak approaching Zhushan and Puli is the latest in NE20 (Fig. 7a). The simulation results in NE50 and NE80 show that the local circulation turns southwesterly earlier so that the tracer is either accumulated near the emission site (Fig. 8h) or transported northward (Fig. 8i) by the circulation of the lee vortex at 18:00 LST. On the other hand, a rather robust westerly over the plain area of central Taiwan in NE20 spreads the TPP tracer to Zhushan and Puli and results in the highest tracer concentration in central Taiwan in the evening (Fig. 8g). With the help of the inactive vertical mixing of the PBL in the evening, the high TPP tracer concentration at Puli at night and its evolution (Fig. 7a) can be further explained using the mixed-layer depth and the local scale downslope winds. Figure 10 shows the vertical cross-section from the coastline to the mountain area at 18:30 LST. The time evolution of the TPP tracer concentration and the local circulation along with the mixed-layer depth is also presented in supplementary material 1. It shows that the timing of the tracer streak across the hill between Zhushan and Puli in NE20 is the latest among all these experiments. As the thinning of mixed-layer depth occurs in the evening, the tracer could be trapped in the Puli basin by the topography. This hypothesis is supported by Fig. 10. The tracer is confined in the Puli basin in NE20 due to the thinning of mixed-layer depth in the evening so that the tracer concentration at Puli is highest among all three experiments.

The results also show that the tracer is transported back and forth on the right (north) slope of the Puli basin after trapping in the basin during the night as presented in Supplementary material 1. It corresponds with the secondary peak of tracer concentration at Puli occurring at around 21:00 LST in NE20 shown in Fig. 7a. The result indicates that the local upslope/downslope wind has to be taken into account when discussing the tracer transport in the complex topography like the Puli basin. While the local circulation in the plain area of central Taiwan is controlled by the lee vortex, the simulated local flow over mountain areas is more turbulent (Figs. 8 and 9), which might indicate that the local upslope/downslope winds over the complex topography could be more dominate. Figure 11 presents the snapshot of the vertical cross-section of tracer transport from TPP along the north slope of the Puli basin (red dotted line in Fig. 1) for NE20 at 08:00 and 20:00 LST. The evolution of the local flow and the tracer concentration is also shown in supplementary material 2. The results show that the diurnal variation of the wind system is consistent with the upslope/downslope wind system in the mountainous area (Whiteman, 2000). The nighttime tracer transport at Puli could be attributed to the downslope wind on the northern slope of the Puli basin. The results suggest that the analysis of the fine structure caused by the local flow over complex topography is necessary to further evaluate its impact on tracer transport.

It is worth noting that the mixed-layer depth over the hilltop is always thinner than it is on the plain or Puli basin the whole time of the simulation. Since the tracer mainly propagates in the boundary layer, the mixed-layer depth can also be a good indication of the horizontal tracer distribution over the mountain area. The thinning of the mixed-layer depth on the mountain area in the evening could prevent tracer transport across the hilltop. This effect results in the opposite scenarios of the SNC tracer transport in NE50 and NE80. The evolution of the SNC tracer concentration and the local circulation along with the mixed-layer depth is presented in supplementary material 3, and snapshots at 18:30 LST for NE50 and NE80 are presented in Fig. 12. The time is selected when the SNC tracer concentration in Zhushan reaches its peak in NE50. As shown in Fig. 7b, the tracer from SNC is transported eastward to Zhushan at 15:30 LST (NE80) and 18:30 LST (NE50). When the tracer streak approaches Zhushan in NE50, the thinning of mixed-layer depth in the evening indicates that the tracer can barely cross the hilltop to the Puli basin. Consequently, the tracer accumulates on the foothill. On the other hand, the tracer from SNC can transport across the hilltop to the Puli basin in the experiment NE80, causing a high concentration of tracer being trapped in the Puli basin.

Figure 13 presents the hovemoller diagram of the surface tracer concentration from SNC and the mixed-layer depth from the coast to the mountain in NE50. The results show that a minimum mixed-layer depth of 250 m is necessary for the tracer to transport across the hill between Zhushan and Puli. The results suggest that the role of PBL development in the tracer transport mechanism is much more important in the mountain area. The local circulation associated with the lee vortex and the diurnal development of the PBL are crucial factors in controlling the distribution of the tracer over complex topography.

5. Summary and Discussion

With the idealized TaiwanVVM simulations performed in this study, the tracer transport and accumulation from coastal emission sources (Taichung Power Plant (TPP) and Sixth Naphtha Cracker (SNC)) to the mountain area (Zhushan and Puli) in central Taiwan are examined. We idealized the wind directions of crucial synoptic weather northeast monsoon as the initial conditions to study the mechanisms responsible for the diurnal evolution of the tracer concentration in Zhushan and Puli. The idealization is based on the observed pollution days in Puli in which the major wind directions are northeasterly due north (NE20), northeasterly (NE50), and northeasterly due east (NE80). The results show that the island-scale circulation associated with the sea breeze and the lee vortex controls the timing of the tracer transport to the front edges of the mountain area in the diurnal time scale. As the tracer approaches the mountain area, the evolution of the PBL also determines whether the tracer could be transported across the hills near Zhushan and Puli and consequently impacts the tracer concentration in Puli at night. Once the tracer transports into the Puli basin, the thinning of the mixed layer depth and the topography could trap the tracer, resulting in a high concentration through the night. The sensitivity of the local tracer transport to the change of the synoptic wind direction shows that in NE80 (NE20), the pollutant transports from SNC (TPP) are most likely to induce high concentrations in Puli at night.

Regarding the local circulation, the simulation results in this study clarified the contribution of the sea breeze and the lee vortex in pollutants transport in central Taiwan. The conclusion provides an insight to interpret the intensification of the westerly in central Taiwan. As the prevailing winds turn from northerly to easterly (described as a larger pitching angle in LL20), the impact of the lee vortex in terms of the robust westerly becomes more profound. In this circumstance, the local circulation is mainly controlled by the evolution of the lee vortex so that the role of the sea breeze in tracer transport is minor. Moreover, the results indicate that the local meridional flow associated with the lee vortex tends to be more transient. It varies following the movement of the lee vortex. It is more challenging to identify the effects of the lee vortex by the composite of the observations or simulations. The design of the experiments in this study provides a novel approach to evaluate the evolution of the interaction between the topography of Taiwan and the prevailing synoptic winds. With only the crucial factors prescribed in the numerical setup of the idealized simulation, the complexity of the reality is trimmed to a more focusing framework so that the response of the local flow to the synoptic condition could be evaluated more precisely. The conclusion in this study also suggests that there could be some information hidden in the variability of the observed meridional component of the local flow, which needs to be further inspected. While the focusing area of this study is in central Taiwan, we believe that the effects of the PBL development on the pollutants transport and accumulation over the mountain area are more general. The mechanism of the tracer transport revealed in this study should be applied to other areas of Taiwan or other islands with complex topography.

Regarding the improvement of the simulation framework, the ongoing work is to implement the chemical processes into this model so that the distribution of the chemical species could be evaluated to better understand the role of chemical reactions during the pollutants transport. Additional idealized simulations will be performed based on soundings at Ishigakijima, such as prevailing wind speed or the strength of the temperature inversion to better understand the variabilities of the lee vortex and the boundary layer processes. The results can be used to construct conceptual models that determine the pollution scenarios at Puli and further establish the foundations of the storyline approach (Shepherd et al., 2018) to study the impact of climate change on the pollution distribution in Taiwan.

Considering that the local $PM_{2.5}$ concentration at Puli is the result of chemical processes and the transport of the pollutants emitted from all the emission sources, it is challenging to clarify the cause of high pollution in Puli. The results obtained from idealized experiments in this study, however, provide possible pathways from the view of pollutants transport. Based on the conclusion of this study, we can propose a tracer transport field experiment in the future to precisely measure the tracer concentrations under the impact of the lee vortex according to the synoptic wind directions. The deployment of the tracer emission and the capture instruments can be arranged across the west plain of Taiwan.

Appendix: A pollution episode in Taiwan with the existence of the lee vortex on March 27th, 2012

Figure A1 shows a snapshot of the $PM_{2.5}$ concentration observations in Taiwan along with the 10 m wind surrounding Taiwan from ERA5 reanalysis datasets (Hersbach et al., 2020) in a pollution episode at 8:00 LST on March 27th, 2012. A lee vortex, which is located on the Taiwan Strait, is accompanied by the high aerosol concentration in central Taiwan under the prevailing easterly. This event provides direct observation evidence of the existence of the lee vortex in the pollution events in Taiwan, which is not discussed in LL20. The observation along with the reanalysis of wind fields support the motivation of this study and inspire the design of the idealized experiments.

Data Availability Statement

The model results of TaiwanVVM used in this study can be made available by contacting the author through the e-mail: miles0919@gmail.com.

Supplement

Supplementary 1 shows the time evolution of the TPP tracer concentration and the local circulation along the vertical cross-section from the coastline to the mountain area in all experiments. Supplementary 2 shows the diurnal evolution of the local flow and the TPP tracer concentration along the north slope of the Puli basin. Supplementary 3 shows the time evolution of the SNC tracer concentration and the local circulation along the vertical cross-section from the coastline to the mountain area in NE50 and NE80.

Acknowledgments

This study is jointly supported by the Ministry of Science and Technology in Taiwan through Grant 107-2111-M-002-010-MY4 and Academia Sinica through Grant AS-TP-109-M11 to National Taiwan University. We appreciate Ms. Tzu-Han Hsu to provide Fig. A1 in this manuscript as the observation evidence of the lee vortex in a pollution event in Taiwan.

References

1. Arakawa, A., Wu, C.-M., 2013. A Unified Representation of Deep Moist Convection in Numerical Modeling of the Atmosphere. Part I. Journal of the Atmospheric Sciences 70, 1977–1992. https://doi.org/10.1175/JAS-D-12-0330.1

2. Arnold, D., Morton, D., Schicker, I., Seibert, P., Rotach, M.W., Horvath, K., Dudhia, J., Satomura, T., Müller, M., Zängl, G., Takemi, T., Serafin, S., Schmidli, J., Schneider, S., 2012a. High Resolution Modelling in Complex Terrain, in: Report on HiRCoT 2012 Workshop. Presented at the HiRCoT 2012 Workshop, Vienna, p. 42.

3. Arnold, D., Morton, D., Schicker, I., Seibert, P., Rotach, M.W., Horvath, K., Dudhia, T., Satomura, T., Müller, M., Zängl, G., Takemi, T., Serafin, S., Schmidli, J., Schneider, S., 2012b. ISSUES IN HIGH-RESOLUTION ATMOSPHERIC MODELING IN COMPLEX TOPOGRAPHY --THE HiRCoT WORKSHOP. Hrvatski meteorološki časopis 47, 3–11.

4. Chang, C.-M., Chang, L.-N., Hsiao, H.-C., Lu, F.-C., Shieh, P.-F., Chen, C.-N., Lu, S.-C., 2006. A Further Study of High Air Pollution Episodes in Taiwan Using the Microwave Temperature Profiler (MTP-5HE). JSME International Journal Series B Fluids and Thermal Engineering 49, 60–64. https://doi.org/10.1299/jsmeb.49.60

5. Chang, Y.-H., Chen, W.-T., Wu, C.-M., Moseley, C., Wu, C.-C., 2021. Tracking the influence of cloud condensation nuclei on summer diurnal precipitating systems over complex topography in Taiwan. Atmospheric Chemistry and Physics Discussions 1–28. https://doi.org/10.5194/acp-2021-113

6. Chen, Y.-T., Wu, C.-M., 2019. The Role of Interactive SST in the Cloud-Resolving Simulations of Aggregated Convection. Journal of Advances in Modeling Earth Systems 11, 3321–3340. https://doi.org/10.1029/2019MS001762

7. Cheng, F.-Y., Chin, S.-C., Liu, T.-H., 2012. The role of boundary layer schemes in meteorological and air quality simulations of the Taiwan area. Atmospheric Environment 54, 714–727. https://doi.org/10.1016/j.atmosenv.2012.01.029

8. Chien, M.-H., Wu, C.-M., 2016. Representation of topography by partial steps using the immersed boundary method in a vector vorticity equation model (VVM): VVM PARTIAL STEP. Journal of Advances in Modeling Earth Systems 8, 212–223. https://doi.org/10.1002/2015MS000514

9. Chuang, M.-T., Chiang, P.-C., Chan, C.-C., Wang, C.-F., Chang, E.-E., Lee, C.-T., 2008. The effects of synoptical weather pattern and complex terrain on the formation of aerosol events in the Greater Taipei area. Science of The Total Environment 399, 128–146. https://doi.org/10.1016/j.scitotenv.2008.01.051

10. Goger, B., Rotach, M.W., Gohm, A., Fuhrer, O., Stiperski, I., Holtslag, A.A.M., 2018. The Impact of Three-Dimensional Effects on the Simulation of Turbulence Kinetic Energy in a Major Alpine Valley. Boundary-Layer Meteorol 168, 1–27. https://doi.org/10.1007/s10546-018-0341-y

11. Goger, B., Rotach, M.W., Gohm, A., Stiperski, I., Fuhrer, O., Morsier, G. de, 2019. A New Horizontal Length Scale for a Three-Dimensional Turbulence Parameterization in Mesoscale Atmospheric Modeling over Highly Complex Terrain. Journal of Applied Meteorology and Climatology 58, 2087–2102. https://doi.org/10.1175/JAMC-D-18-0328.1

12. Hersbach, H., Bell, B., Berrisford, P., Hirahara, S., Horányi, A., Muñoz-Sabater, J., Nicolas, J., Peubey, C., Radu, R., Schepers, D., Simmons, A., Soci, C., Abdalla, S., Abellan, X., Balsamo, G., Bechtold, P., Biavati, G., Bidlot, J., Bonavita, M., De Chiara, G., Dahlgren, P., Dee, D., Diamantakis, M., Dragani, R., Flemming, J., Forbes, R., Fuentes, M., Geer, A., Haimberger, L., Healy, S., Hogan, R.J., Hólm, E., Janisková, M., Keeley, S., Laloyaux, P., Lopez, P., Lupu, C., Radnoti, G., de Rosnay, P., Rozum, I., Vamborg, F., Villaume, S., Thépaut, J.-N., 2020. The ERA5 global reanalysis. Quarterly Journal of the Royal Meteorological Society 146, 1999–2049. https://doi.org/10.1002/qj.3803.

13. Hsu, C.-H., Cheng, F.-Y., 2019. Synoptic Weather Patterns and Associated Air Pollution in Taiwan. Aerosol Air Qual. Res. 19, 1139–1151. https://doi.org/10.4209/aaqr.2018.09.0348

14. Hsu, C.-H., Cheng, F.-Y., 2016. Classification of weather patterns to study the influence of meteorological characteristics on PM2.5 concentrations in Yunlin

County, Taiwan. Atmospheric Environment 144, 397–408. https://doi.org/10.1016/j.atmosenv.2016.09.001

15. Jung, J.-H., Arakawa, A., 2008. A Three-Dimensional Anelastic Model Based on the Vorticity Equation. Mon. Wea. Rev. 136, 276–294. https://doi.org/10.1175/2007MWR2095.1

16. Kuo, K.-T., Wu, C.-M., 2019. The Precipitation Hotspots of Afternoon Thunderstorms over the Taipei Basin: Idealized Numerical Simulations. Journal of the Meteorological Society of Japan. Ser. II 97, 501–517. https://doi.org/10.2151/jmsj.2019-031

17. Lai, H.-C., Lin, M.-C., 2020. Characteristics of the upstream flow patterns during PM2.5 pollution events over a complex island topography. Atmospheric Environment 227, 117418. https://doi.org/10.1016/j.atmosenv.2020.117418

18. Lesouëf, D., F, G., Delmas, R., Escobar, J., 2011. Numerical simulations of local circulations and pollution transport over Reunion Island. Annales Geophysicae 29. https://doi.org/10.5194/angeo-29-53-2011

19. Shepherd, T.G., Boyd, E., Calel, R.A., Chapman, S.C., Dessai, S., Dima-West, I.M., Fowler, H.J., James, R., Maraun, D., Martius, O., Senior, C.A., Sobel, A.H., Stainforth, D.A., Tett, S.F.B., Trenberth, K.E., van den Hurk, B.J.J.M., Watkins, N.W., Wilby, R.L., Zenghelis, D.A., 2018. Storylines: an alternative approach to

representing uncertainty in physical aspects of climate change. Climatic Change 151, 555–571. https://doi.org/10.1007/s10584-018-2317-9

20. Tsai, H.H., Ti, T.H., Yuan, C.-S., Hung, C.-H.J., Lin, C., 2008. Effects of Sea-Land Breezes on the Spatial and Temporal Distribution of Gaseous Air Pollutants at the Coastal Region of Southern Taiwan. J. Environ. Eng. Manag. 18, 387–396.

21. Tsai, J.-Y., Wu, C.-M., 2016. Critical transitions of stratocumulus dynamical systems due to perturbation in free-atmosphere moisture. Dynamics of Atmospheres and Oceans 76, 1–13. https://doi.org/10.1016/j.dynatmoce.2016.08.002

22. Tsai, W.-M., Wu, C.-M., 2017. The environment of aggregated deep convection. Journal of Advances in Modeling Earth Systems 9, 2061–2078. https://doi.org/10.1002/2017MS000967

23. Whiteman, C.D., 2000. Mountain Meteorology: Fundamentals and Applications. Oxford University Press.

24. Wu, C.-M., Arakawa, A., 2014. A Unified Representation of Deep Moist Convection in Numerical Modeling of the Atmosphere. Part II. Journal of the Atmospheric Sciences 71, 2089–2103. https://doi.org/10.1175/JAS-D-13-0382.1

25. Wu, C.-M., Arakawa, A., 2011. Inclusion of Surface Topography into the Vector Vorticity Equation Model (VVM): INCLUSION OF SURFACE TOPOGRAPHY

INTO THE VVM. Journal of Advances in Modeling Earth Systems 3, n/a-n/a. https://doi.org/10.1029/2011MS000061

26. Wu, C.-M., Lin, H.-C., Cheng, F.-Y., Chien, M.-H., 2019. Implementation of the Land Surface Processes into a Vector Vorticity Equation Model (VVM) to Study its Impact on Afternoon Thunderstorms over Complex Topography in Taiwan. Asia-Pacific J Atmos Sci 55, 701–717. https://doi.org/10.1007/s13143-019-00116-x

List of Figures

Fig. 1 The geographic locations of Taiwan and Ishigakijima of Japan, and the sites of the tracer emission and the concentration to be examined in central Taiwan based on the topography used in TaiwanVVM. The red squares represent emission sites at Taipower Power Plant (TPP) and Sixth Naphtha Cracker (SNC), which are major non-traffic emission sites on the west coast of Taiwan. The blue triangles mark the local $PM_{2.5}$ observation sites and the simulated tracer concentration we examined. The thin line following the topography is the contour of 700 m height above the sea level, which shows the geographic situation of the Puli basin. The black dashed line and the red dotted line represent the cross-section of the vertical circulation and the tracer transport examined in this study.

Fig. 2 The windroses of the synoptic winds in (a) all days and (b) pollution days at Puli in 2005-2015. The number on the windroses represents percentages of the events. The wind of the lowest level in the sounding data at Ishigakijima of Japan at 00:00 UTC of the day is taken to represent the synoptic winds. The definition of the pollution day at Puli is that the daily mean $PM_{2.5}$ concentration exceeds 54.5 μg m^{-3}, described as unhealthy by the EPA of Taiwan.

Fig. 3 The diurnal evolution of the (a) $PM_{2.5}$ concentration, (b) zonal wind, and (c) meridional wind at Zhushan and Puli in 310 pollution days at Puli from 2005 to 2015. The red(blue) lines and shaded areas present the composite of the 310 cases and its standard deviation at Puli(Zhushan).

Fig. 4 The initial (a) potential temperature, (b) water vapor mixing ratio, and wind profiles in (c) NE20, (d) NE50, and (e) NE80 experiments. The initial potential temperature and moisture profiles of all experiments (red lines in subfigures (a) and (b)) are idealized from the sounding data at Ishigakijima of Japan at 00 UTC on Dec. 21, 2017 (blue lines in subfigures (a) and (b)). The initial wind direction below 850 m (red dashed lines in subfigures (c) (d) (e)) are set to 20°, 50°, and 80° in (c) NE20, (d) NE50, and (e) NE80, respectively.

Fig. 5 The streamlines of the 10 m wind associated with the lee vortex at 12:00 LST for (a) NE20, (b) NE50 and (c) NE80 and at 22:00 LST for (d)NE20, (e) NE50 and (f) NE80.

Fig. 6 The evolution of the (a) zonal component and (b) meridional component of the mean 10 m wind in the plain area of central Taiwan. The red, green, and blue lines represent the wind speed in experiments NE20, NE50, and NE80. The plain area of central Taiwan is defined as the grid points over land where the elevation is less than 200 m in the domain of Fig. 1.

Fig. 7 The time evolution of the local tracer concentration emitted from (a) TPP and (b) SNC in the experiments. The solid (dash) lines represent the concentration at Puli (Zhushan). The red, green, and blue lines represent concentration in experiments NE20, NE50, and NE80. The timing of the highest concentration at Zhushan and Puli is also shown in the figure.

Fig. 8 The near-surface concentration and the 10 m wind evolution of the tracer emitted from TPP in three experiments. The green-colored shading represents the topography of Taiwan. The streamlines represent the near-surface flow as defined in Fig. 6. The flow pattern and the tracer concentration are shown in (a) NE20, (b) NE50, and (c) NE80 at 11:00 LST. The subfigures (d) (e) (f) and (g) (h) (i) present the flow patterns and the tracer concentration for all experiments at 14:00 and 18:00LST, respectively. The near-surface concentration is defined as the concentration at the lowest model level above the surface.

Fig. 9 Similar to Fig. 8 except for the tracer emitted from SNC.

Fig. 10 The vertical cross-section of tracer concentration from TPP and the local circulation at 18:30 LST along the black dashed line in Fig. 1 in experiments (a) NE20, (b) NE50, and (c) NE80. The red dashed lines represent the mixing layer depth.

Fig. 11 The vertical cross-section of the TPP tracer concentration and the mountain-valley wind circulation at the north slope of Puli basin (the red dotted line shown in Fig. 1) in experiment NE20. Subfigures (a) and (b) represent the concentration and the circulation at 08:00 LST and 20:00 LST. The black dashed lines represent the mixing layer depth.

Fig. 12 The vertical cross-section of SNC tracer concentration and the local circulation at 18:30 LST along the black dashed line in Fig. 1 in experiments (a) NE50 and (b) NE80. The red dashed lines represent the mixing layer depth.

Fig. 13 The hovemuller diagram of the surface SNC tracer concentration and the mixed-layer depth along the dashed line in Fig. 1 in NE50. The hatched patches represent the areas in which the mixed-layer depth is thinner than 250 m.

Fig. A1 The $PM_{2.5}$ concentration of Taiwan and the 10 m wind field around Taiwan in a pollution episode at 8:00 LST on March 27th, 2012. The wind field is obtained from the ERA5 reanalysis dataset.

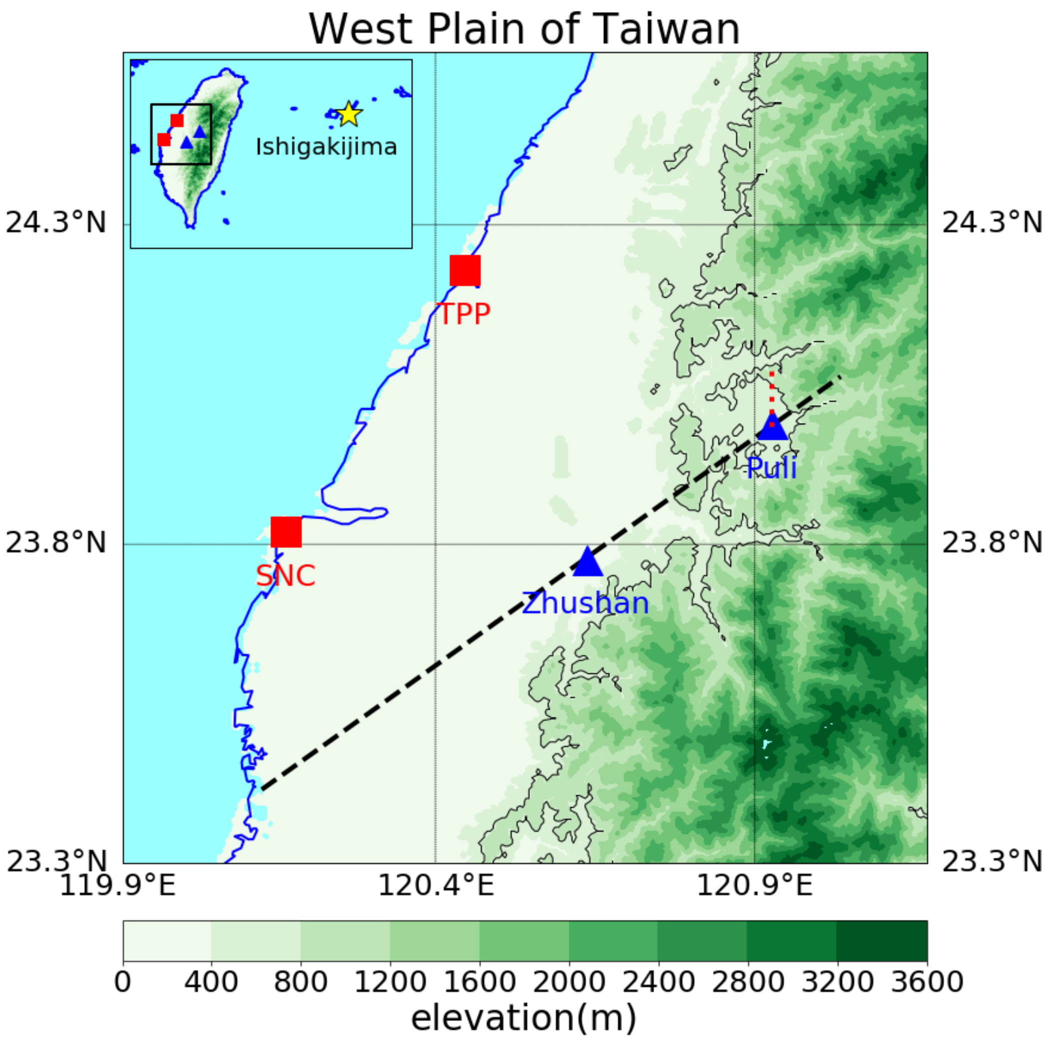

Fig. 1 The geographic locations of Taiwan and Ishigakijima of Japan, and the sites of the tracer emission and the concentration to be examined in central Taiwan based on the topography used in TaiwanVVM. The red squares represent emission sites at Taipower Power Plant (TPP) and Sixth Naphtha Cracker (SNC), which are major non-traffic emission sites on the west coast of Taiwan. The blue triangles mark the local $PM_{2.5}$ observation sites and the simulated tracer concentration we examined. The thin line following the topography is the contour of 700 m height above the sea level, which shows the geographic situation of the Puli basin. The black dashed line and the red

dotted line represent the cross-section of the vertical circulation and the tracer transport examined in this study.

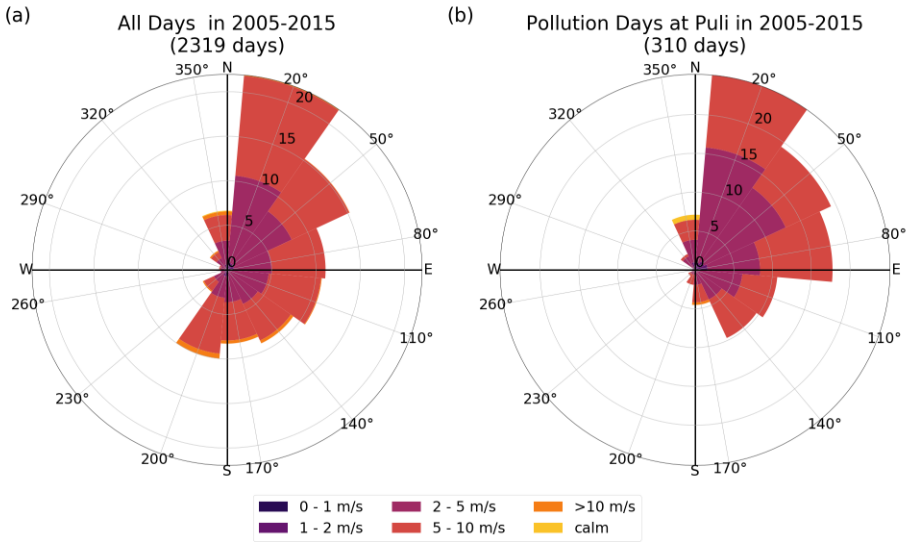

Fig. 2 The windroses of the synoptic winds in (a) all days and (b) pollution days at Puli in 2005-2015. The number on the windroses represents percentages of the events. The wind of the lowest level in the sounding data at Ishigakijima of Japan at 00:00 UTC of the day is taken to represent the synoptic winds. The definition of the pollution day at Puli is that the daily mean $PM_{2.5}$ concentration exceeds 54.5 μg m^{-3}, described as unhealthy by the EPA of Taiwan.

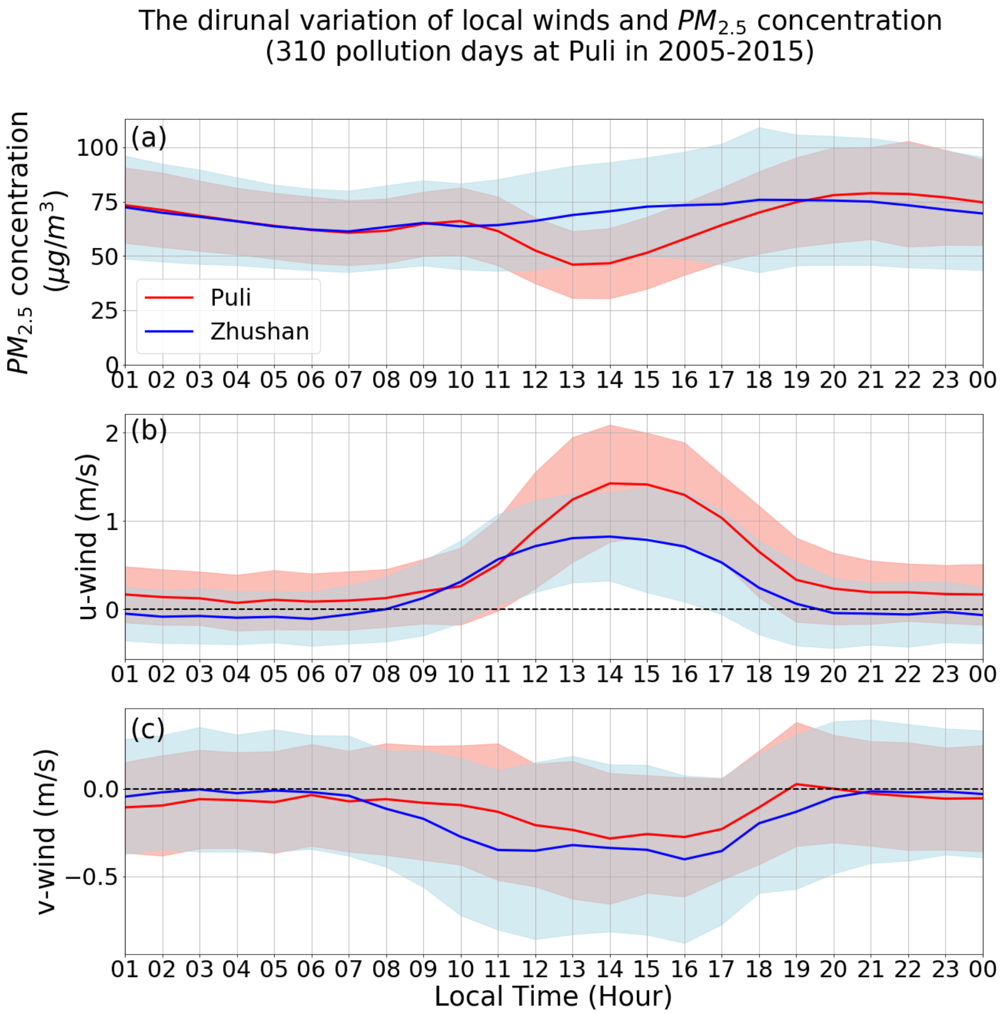

Fig. 3 The diurnal evolution of the (a) $PM_{2.5}$ concentration, (b) zonal wind, and (c) meridional wind at Zhushan and Puli in 310 pollution days at Puli from 2005 to 2015. The red(blue) lines and shaded areas present the composite of the 310 cases and its standard deviation at Puli(Zhushan).

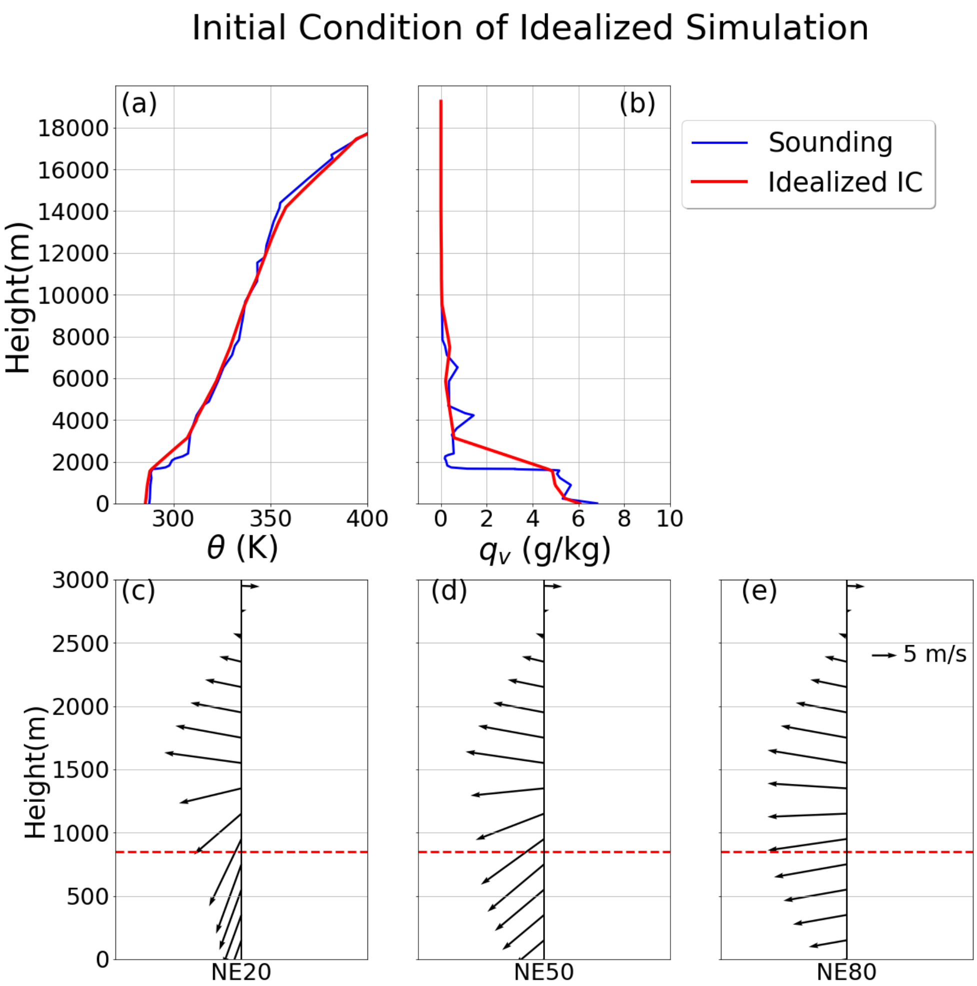

Fig. 4 The initial (a) potential temperature, (b) water vapor mixing ratio, and wind profiles in (c) NE20, (d) NE50, and (e) NE80 experiments. The initial potential temperature and moisture profiles of all experiments (red lines in subfigures (a) and (b)) are idealized from the sounding data at Ishigakijima of Japan at 00 UTC on Dec. 21, 2017 (blue lines in subfigures (a) and (b)). The initial wind direction below 850 m (red dashed lines in subfigures (c) (d) (e)) are set to 20°, 50°, and 80° in (c) NE20, (d) NE50, and (e) NE80, respectively.

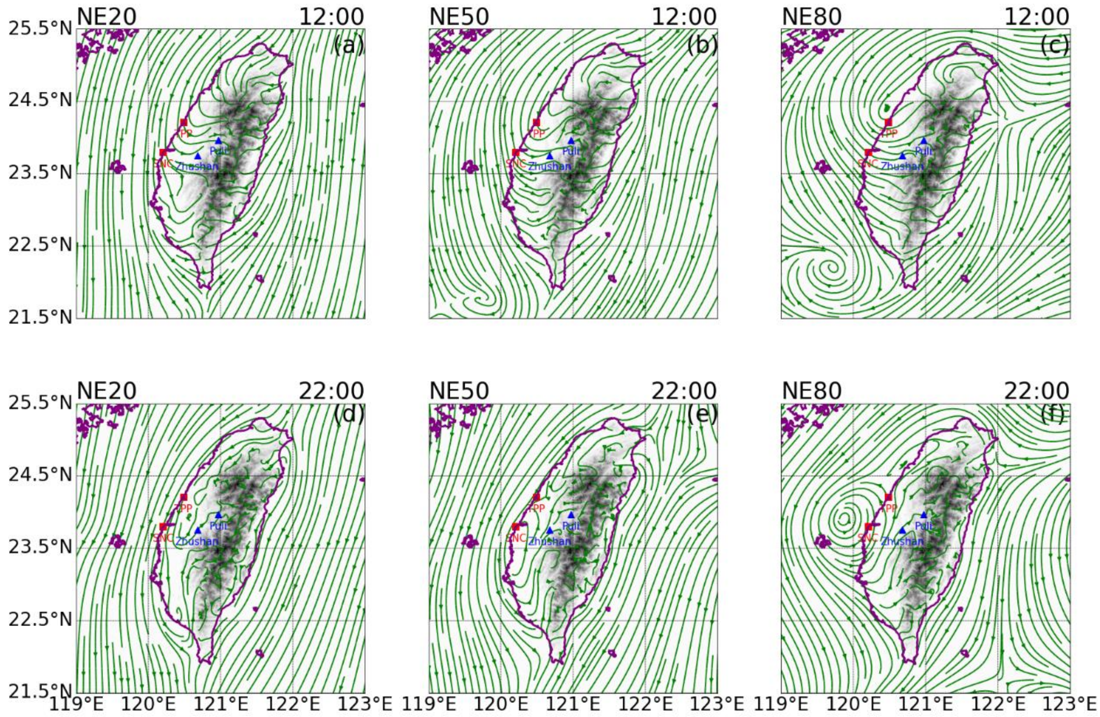

Fig. 5 The streamlines of the 10 m wind associated with the lee vortex at 12:00 LST for (a) NE20, (b) NE50 and (c) NE80 and at 22:00 LST for (d)NE20, (e) NE50 and (f) NE80.

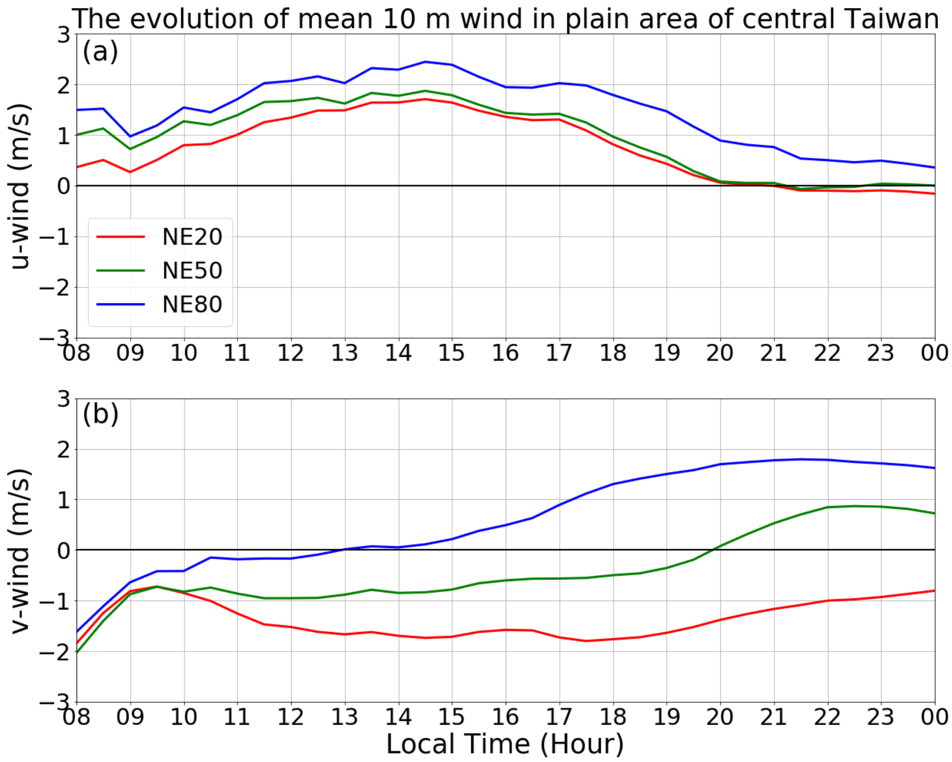

Fig. 6 The evolution of the (a) zonal component and (b) meridional component of the mean 10 m wind in the plain area of central Taiwan. The red, green, and blue lines represent the wind speed in experiments NE20, NE50, and NE80. The plain area of central Taiwan is defined as the grid points over land where the elevation is less than 200 m in the domain of Fig. 1.

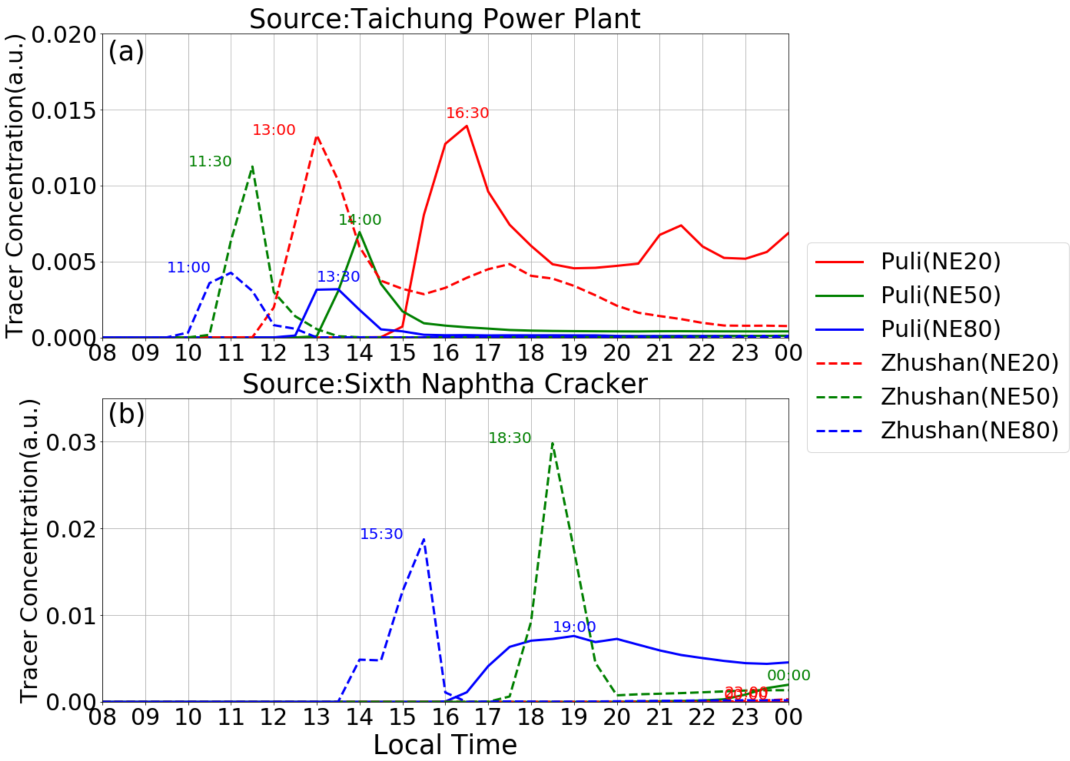

Fig. 7 The time evolution of the local tracer concentration emitted from (a) TPP and (b) SNC in the experiments. The solid (dash) lines represent the concentration at Puli (Zhushan). The red, green, and blue lines represent concentration in experiments NE20, NE50, and NE80. The timing of the highest concentration at Zhushan and Puli is also shown in the figure.

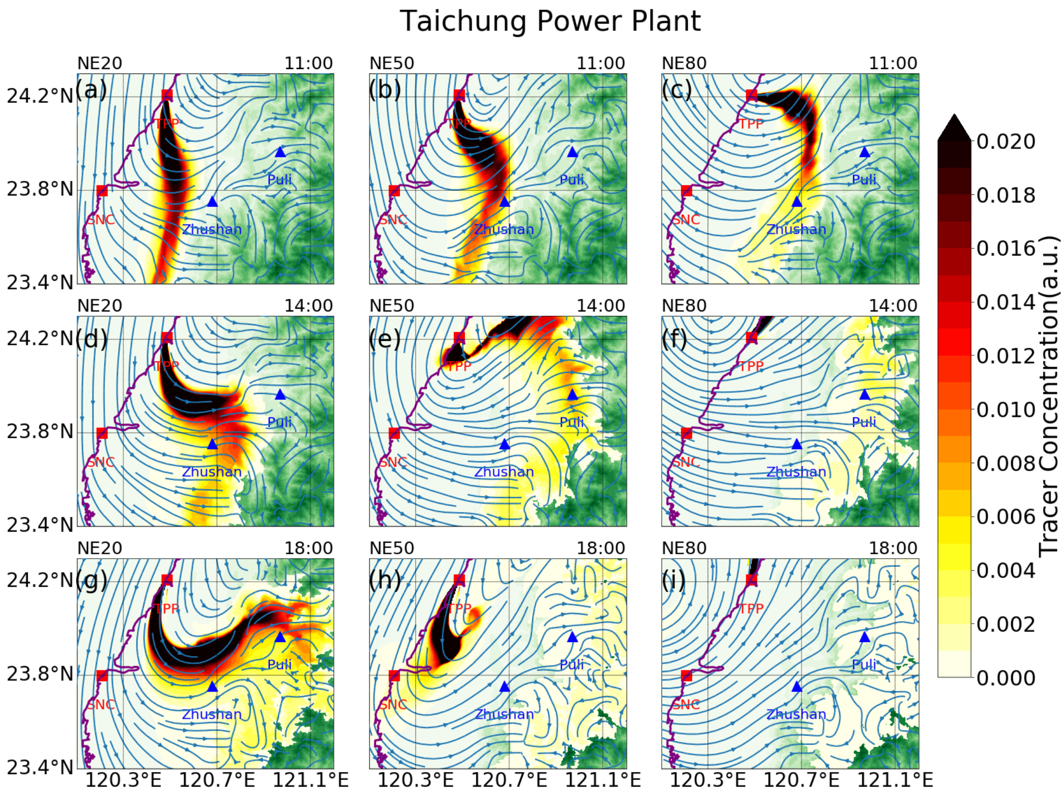

Fig. 8 The near-surface concentration and the 10 m wind evolution of the tracer emitted from TPP in three experiments. The green-colored shading represents the topography of Taiwan. The streamlines represent the near-surface flow as defined in Fig. 6. The flow pattern and the tracer concentration are shown in (a) NE20, (b) NE50, and (c) NE80 at 11:00 LST. The subfigures (d) (e) (f) and (g) (h) (i) present the flow patterns and the tracer concentration for all experiments at 14:00 and 18:00LST, respectively. The near-surface concentration is defined as the concentration at the lowest model level above the surface.

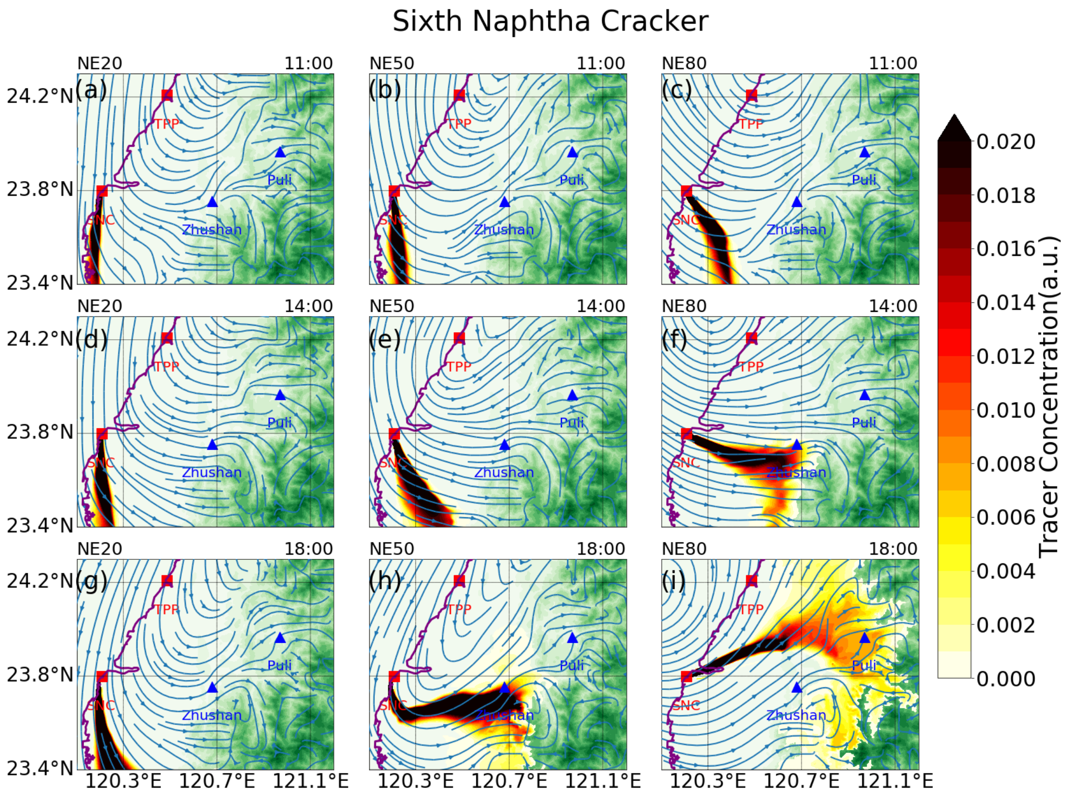

Fig. 9 Similar to Fig. 8 except for the tracer emitted from SNC.

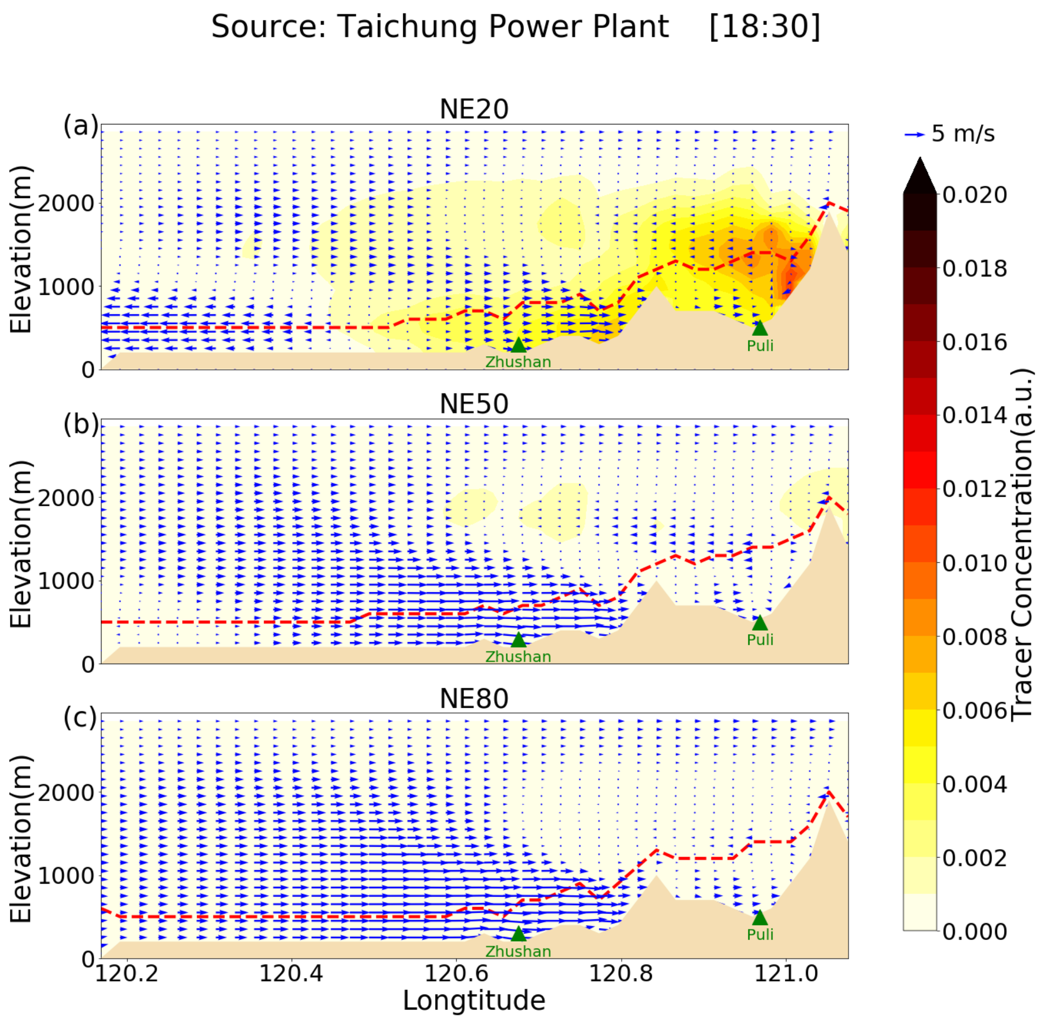

Fig. 10 The vertical cross-section of tracer concentration from TPP and the local circulation at 18:30 LST along the black dashed line in Fig. 1 in experiments (a) NE20, (b) NE50, and (c) NE80. The red dashed lines represent the mixing layer depth.

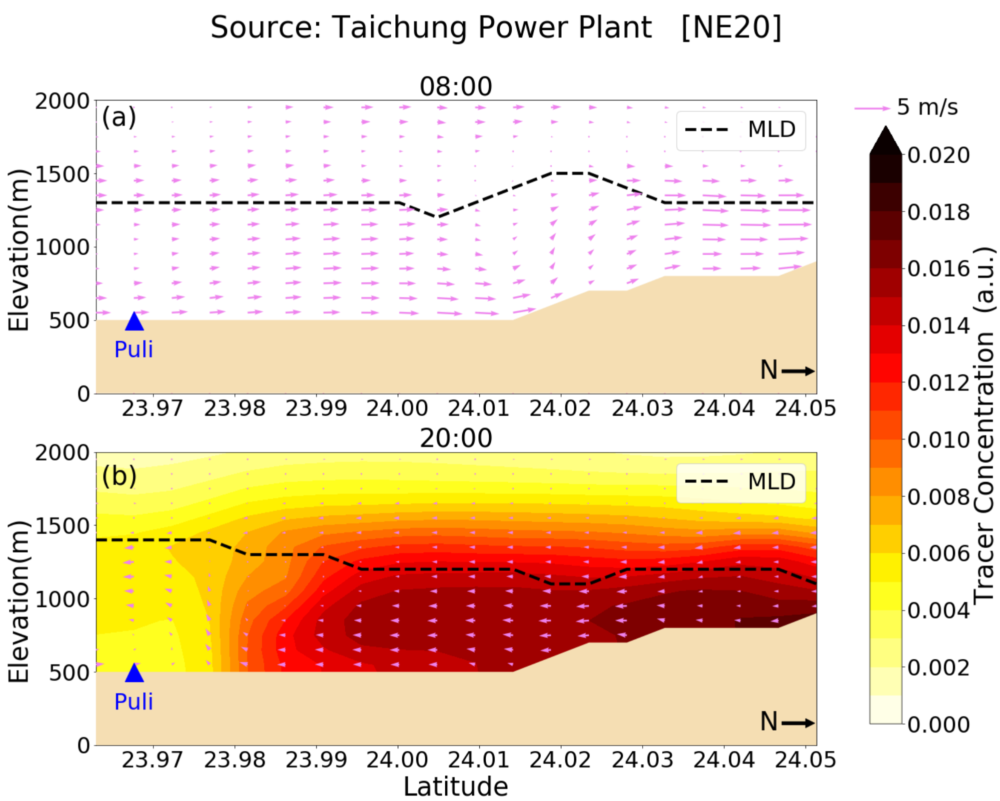

Fig. 11 The vertical cross-section of the TPP tracer concentration and the mountain-valley wind circulation at the north slope of Puli basin (the red dotted line shown in Fig. 1) in experiment NE20. Subfigures (a) and (b) represent the concentration and the circulation at 08:00 LST and 20:00 LST. The black dashed lines represent the mixing layer depth.

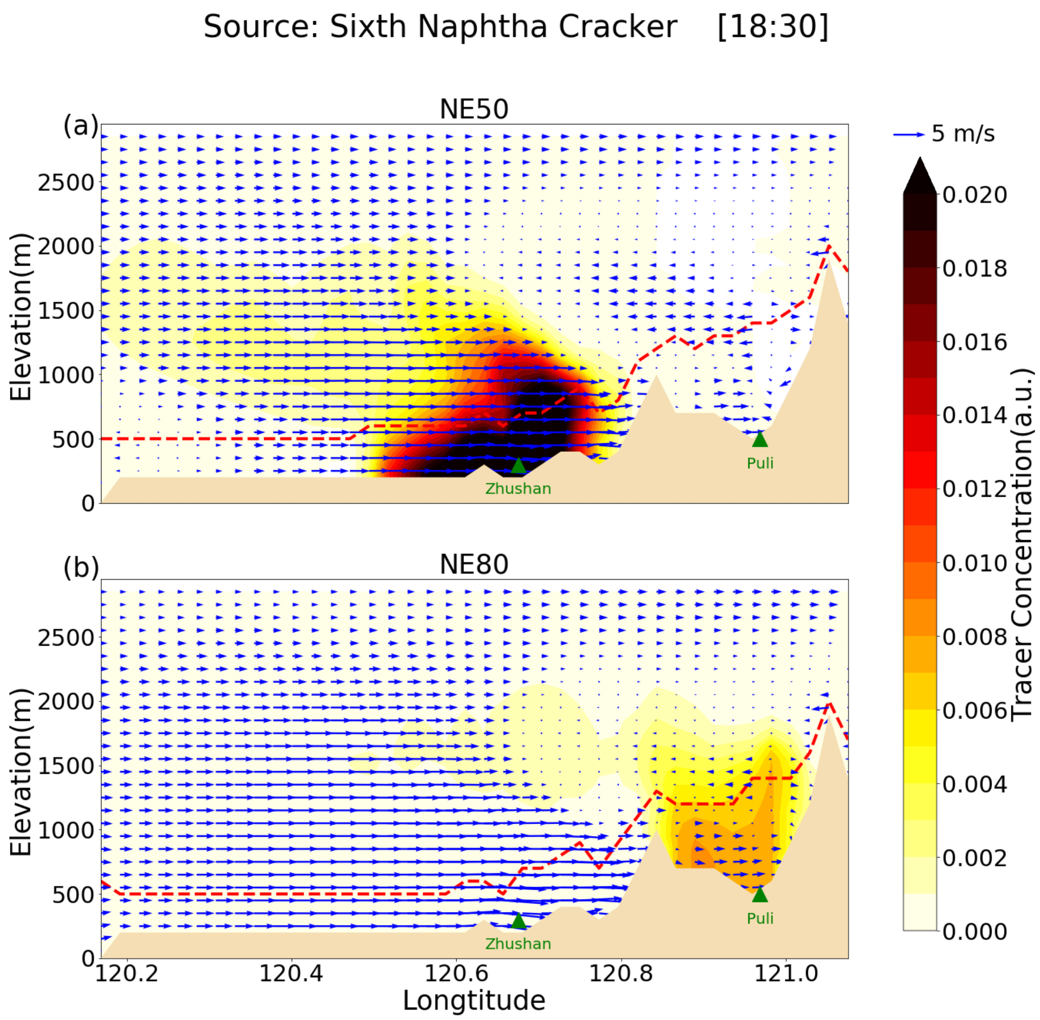

Fig. 12 The vertical cross-section of SNC tracer concentration and the local circulation at 18:30 LST along the black dashed line in Fig. 1 in experiments (a) NE50 and (b) NE80. The red dashed lines represent the mixing layer depth.

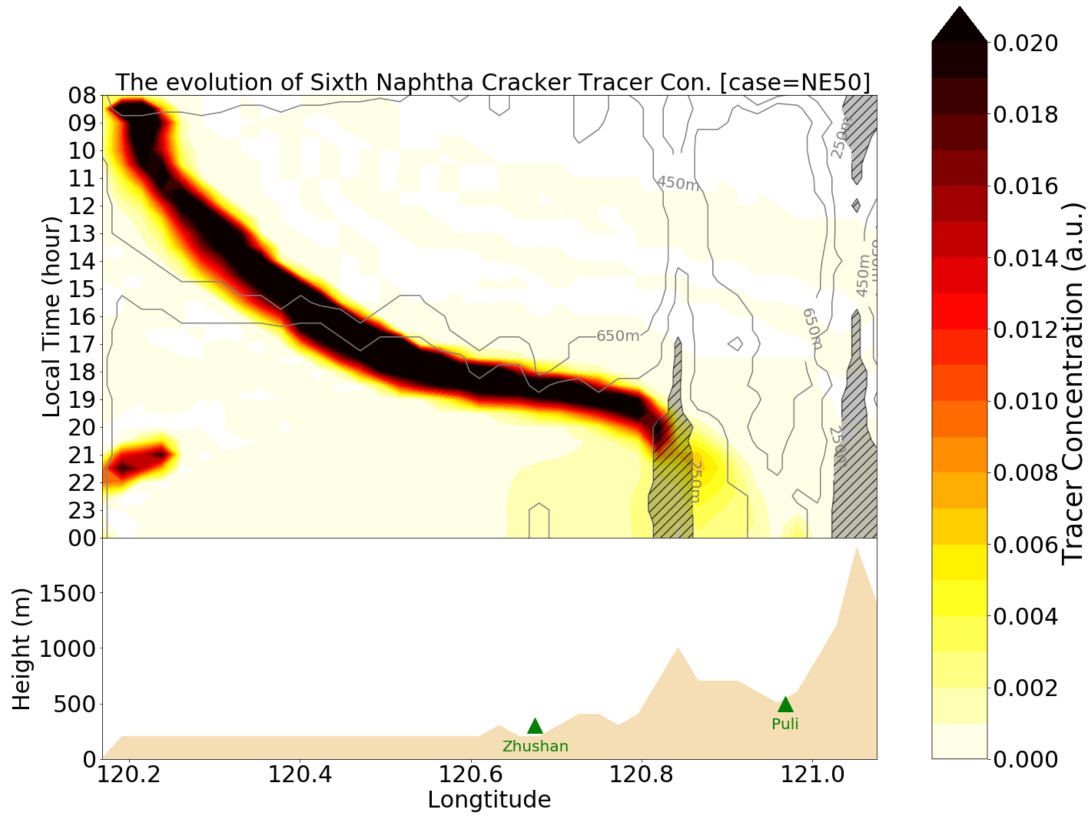

Fig. 13 The hovemuller diagram of the surface SNC tracer concentration and the mixed-layer depth along the dashed line in Fig. 1 in NE50. The hatched patches represent the areas in which the mixed-layer depth is thinner than 250 m.

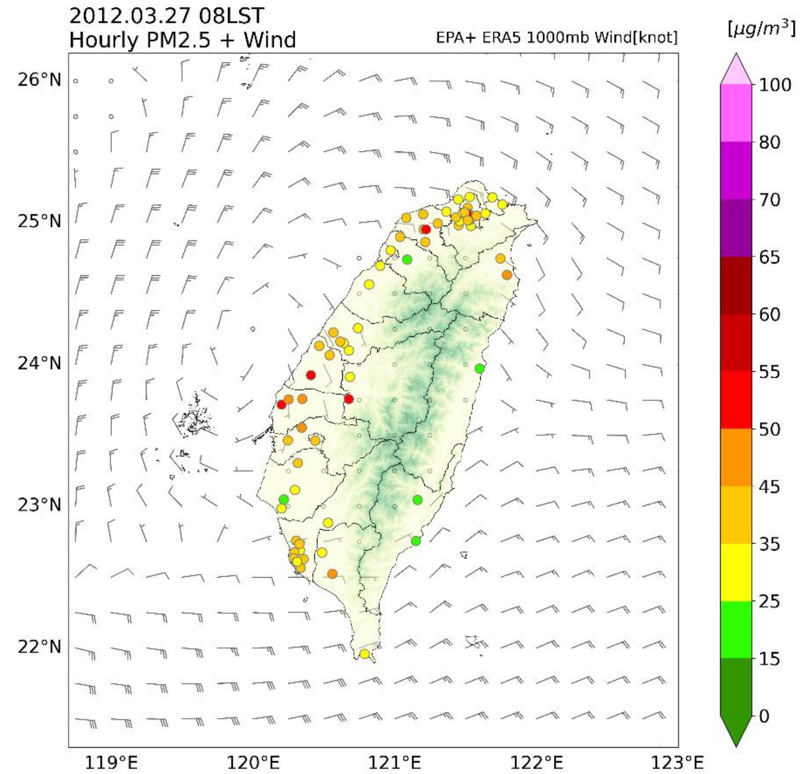

Fig. A1 The $PM_{2.5}$ concentration of Taiwan and the 10 m wind field around Taiwan in a pollution episode at 8:00 LST on March 27th, 2012. The wind field is obtained from the ERA5 reanalysis dataset.

List of Tables

Table 1. The setup of TaiwanVVM simulation

Horizontal Resolution	500 m
Vertical Resolution	100 m under 3900 m Stretch up to 914 m at model top
Domain	1024 × 1024 × 70 grids 512 km × 512 km × 19260 m
Time Step	10 seconds
Simulation Duration	18 h (06:00 – 24:00)
Lateral Boundary Condition	Double periodic